Supporting Information to

Spin-Crossover in a Pseudo-Tetrahedral Bis(Formazanate) Iron Complex

Raquel Travieso-Puente[†] J. O. P. Broekman,[†] Mu-Chieh Chang,[†] Serhiy Demeshko,[‡] Franc Meyer[‡] and Edwin Otten[*,†]

[†] Stratingh Institute for Chemistry, University of Groningen
Nijenborgh 4, 9747 AG Groningen, The Netherlands

[‡] Institut für Anorganische Chemie, Georg-August-Universität Göttingen
Tammannstraße 4, 37077 Göttingen, Germany

Contents

Experimental Section

General Considerations. All manipulations were carried out under nitrogen atmosphere using standard glovebox, Schlenk, and vacuum-line techniques. Toluene and hexane (Aldrich, anhydrous, 99.8%) were passed over columns of Al_2O_3 (Fluka), BASF R3-11-supported Cu oxygen scavenger, and molecular sieves (Aldrich, 4 Å). THF (Aldrich, anhydrous, 99.8%) was dried by percolation over columns of Al_2O_3 (Fluka). Deuterated solvents were vacuum transferred from Na/K alloy (C_6D_6, toluene-d_8, THF-d_8 Euriso-top) and stored under nitrogen. The compound K[PhNNC(*p*-tol)NNPh]·2THF was prepared according to the literature procedure.[1] Anhydrous $FeCl_2$ (Aldrich, 98%) and Bu_4NBr (Sigma-Aldrich, 99%) were used as received.

NMR spectra were recorded on Varian Gemini 200, VXR 300, Mercury 400 or Varian 500 spectrometers. The ^1H and ^{13}C NMR spectra were referenced internally using the residual solvent resonances and reported in ppm relative to TMS (0 ppm); *J* is reported in Hz. Assignment of NMR resonances was aided by gradient-selected COSY, NOESY, HSQC and/or HMBC experiments using standard pulse sequences. Electrochemical measurements were performed under an inert N_2 atmosphere in a glove box using an Autolab PGSTAT 100 computer-controlled potentiostat. Cyclic voltammetry (CV) was performed using a three-electrode configuration comprising of a Pt wire counter electrode, a Ag wire pseudoreference electrode and a Pt disk working electrode (CHI102, CH Instruments, diameter = 2 mm). The Pt working electrode was polished before experiment using alumina slurry (0.05 µm), rinsed with distilled water and subjected to brief ultrasonication to remove any adhered alumina microparticles. The electrodes were then dried in an oven at 75 °C overnight to remove any residual traces of water. The CV data was calibrated by adding ferrocene in THF solution at the end of experiments. In all cases, there is no indication that addition of ferrocene influences the electrochemical behaviour of products. All electrochemical measurements were performed at ambient temperatures under an inert N_2 atmosphere in THF containing 0.1 M $[nBu_4N][PF_6]$ as the supporting electrolyte. Data were recorded with Autolab NOVA software (v.1.8). UV-Vis spectra were recorded in THF solution (~ 10^{-5} M) using a Avantes AvaSpec 3648 spectrometer and AvaLight-DHS lightsource inside a N_2 atmosphere glovebox. EPR spectra were collected on a Bruker ECS 106 spectrometer either at room temperature or at 77 K by freezing the sample in liquid nitrogen inside a finger dewar.

Elemental analyses were performed at Kolbe Microanalytical Laboratory (Mülheim an der Ruhr, Germany) or at the analytical department at Georg-August-Universität Göttingen.

Synthesis of Fe(PhNN(*p*-tol)NNPh)$_2$ (1). To an intense violet solution of K[PhNNC(*p*-tol)NNPh]·2THF (2.32 g, 4.68 mmol) in 60 mL of THF, $FeCl_2$ (297 mg, 2.34 mmol) was added. After stirring at room temperature overnight, the volatiles were removed under vacuo and the residue was subsequently extracted three times with 100 mL of toluene to give a burgundy solution. After concentrating the toluene solution to 10 mL, 30 mL of hexane was added which resulted in precipitation of some of the product. The mixture was heated to dissolve all solid material. Slow cooling of this solution to room temperature afforded compound **1** as dark red crystalline material. Suitable crystals for single crystal X-ray analysis were obtained by slow diffusion of hexane into a toluene solution of 1. (1.00 g, 1.47 mmol,

63%). ^{1}H NMR (C_6D_6, 25 ºC, 400 MHz): δ 10.40 (4H, Ph *o*-CH), 10.15 (2H, *p*-tolyl *m*-CH), 8.06 (3H, *p*-tolyl CH_3), 5.42 (2H, *p*-tolyl *o*-CH), 2.75 (2H, Ph *p*-CH), 1.66 (4H, Ph *m*-CH). ^{13}C NMR (C_6D_6, 400 MHz): δ 242.8 (Ph *o*-C), 180.4 (*p*-tolyl *o*-C), 171.5 (*p*-tolyl *p*-C), 167.1 (Ph *p*-C), 121.5 (Ph *m*-C), 106.9 (*p*-tolyl *m*-C), 80.1 (*p*-tolyl *ipso*-C), 10.2 (*p*-tolyl *p*-CH_3). Anal. calcd. for $C_{40}H_{34}N_8Fe$: C 70.38, H 5.02, N 16.42; found: C 70.27, H 5.12, N 16.37.

Synthesis of [Bu_4N][Fe(PhNN(*p*-tol)NNPh)$_2$] (2). To a burgundy THF solution of **1** (233 mg, 0.342 mmol), NBu_4Br (125 mg, 0.387 mmol) and Na/Hg (2.447 wt% Na, 320.7 mg, 0.342 mmol) were added. After stirring at room temperature overnight, the volatiles were removed under vacuo. The residue was extracted into THF (3 x 15 mL) to give an intensely red solution. Removal of all volatiles and subsequent washing with toluene resulted in **2** as a dark powder (285 mg, 0.308 mmol, 90%). Crystals suitable for X-ray analysis were obtained in virtually quantitative yield by slow diffusion of hexane into a THF solution of **2**. Anal. calcd. for $C_{56}H_{70}N_9Fe{\cdot}2THF$: C 71.89, H 8.11, N 11.79; found: C 71.93, H 7.69, N 11.27.

Analysis of temperature dependence of ^{1}H NMR shifts in compound 1

The temperature dependence of the ^{1}H NMR shifts was modelled according to the ideal solution model (equation 1)[2] using Wolfram Mathematica 10.

(eq 1)
$$\delta_{obs} = \delta_{LS} + \frac{C}{T\left(1+e^{\left(\frac{\Delta H}{RT}-\frac{\Delta S}{R}\right)}\right)}$$

For each of the 6 ^{1}H resonances, the data were fit using as fitting parameters *C*, ΔH and ΔS; the chemical shift in the low-spin state (δ_{LS}) was constrained to the value found in the diamagnetic zinc analogue.[3] Fitting the data with δ_{LS} as one of the fitting parameters results in thermodynamic parameters that are identical within experimental error. These 6 individual values of ΔH and ΔS were then averaged, and the standard deviation was taken, to give the ΔH and ΔS of 22.2(3) kJ·mol^{-1} and 64(1) J·mol^{-1}·K^{-1}, respectively. The data points and fitted lines are shown in Figure 1 of the main text.

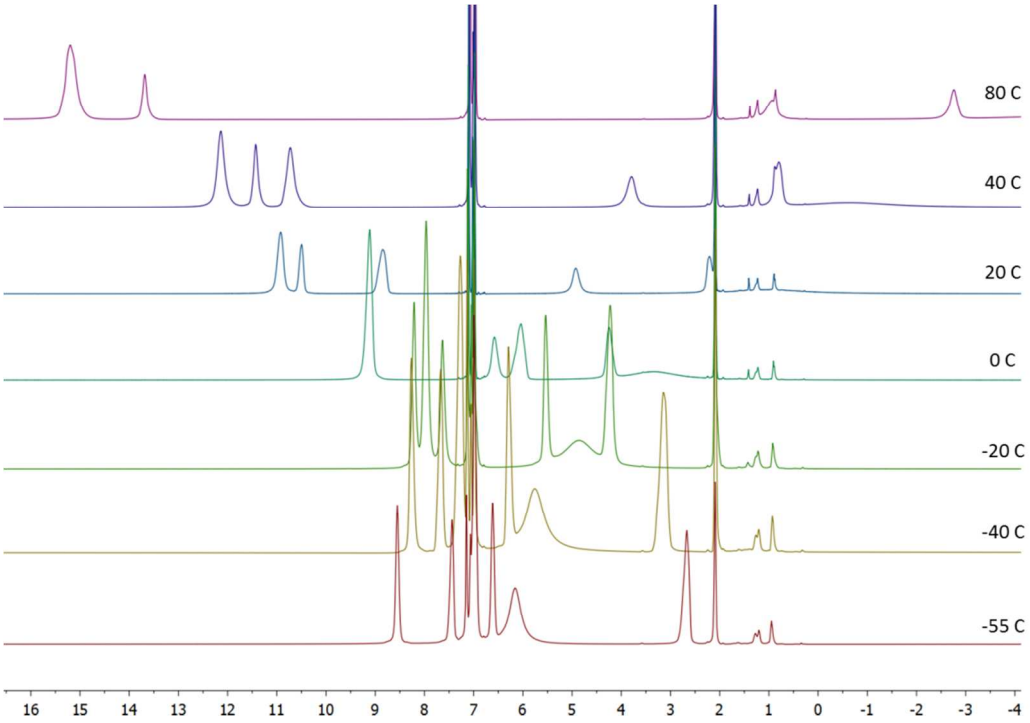

Figure S1. ^{1}H NMR spectra of **1** between -55 and + 80 °C (toluene-d_8 solution).

2D-NMR spectra of compound 1

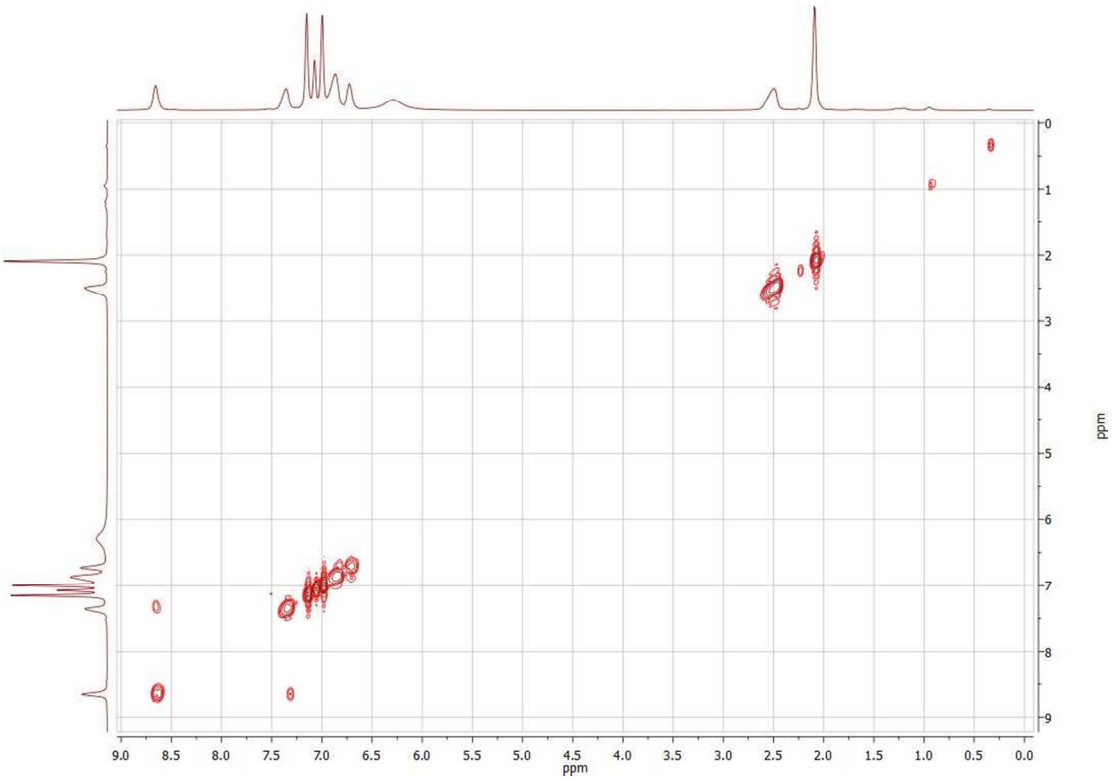

Figure S2. gCOSY NMR spectra of **1** at -60 °C (toluene-d_8 solution).

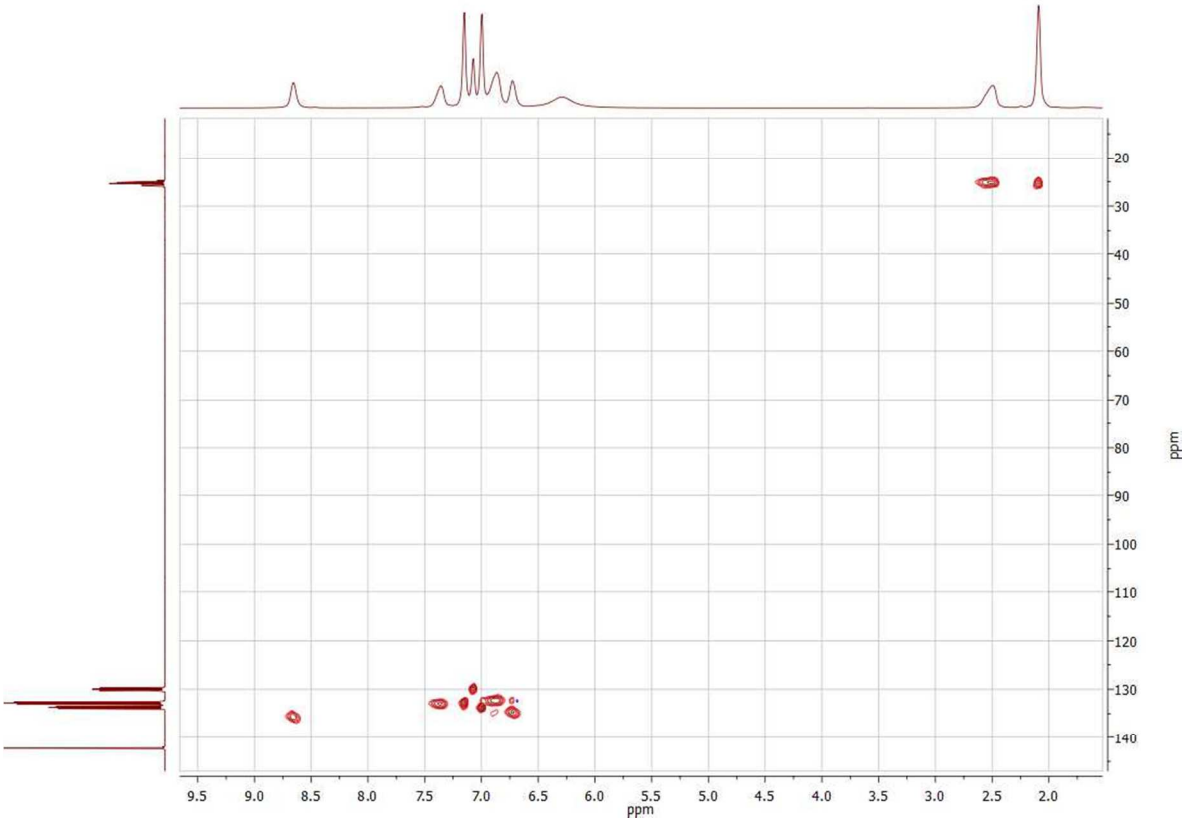

Figure S3. gHSQC NMR spectra of **1** at -60 °C (toluene-d_8 solution).

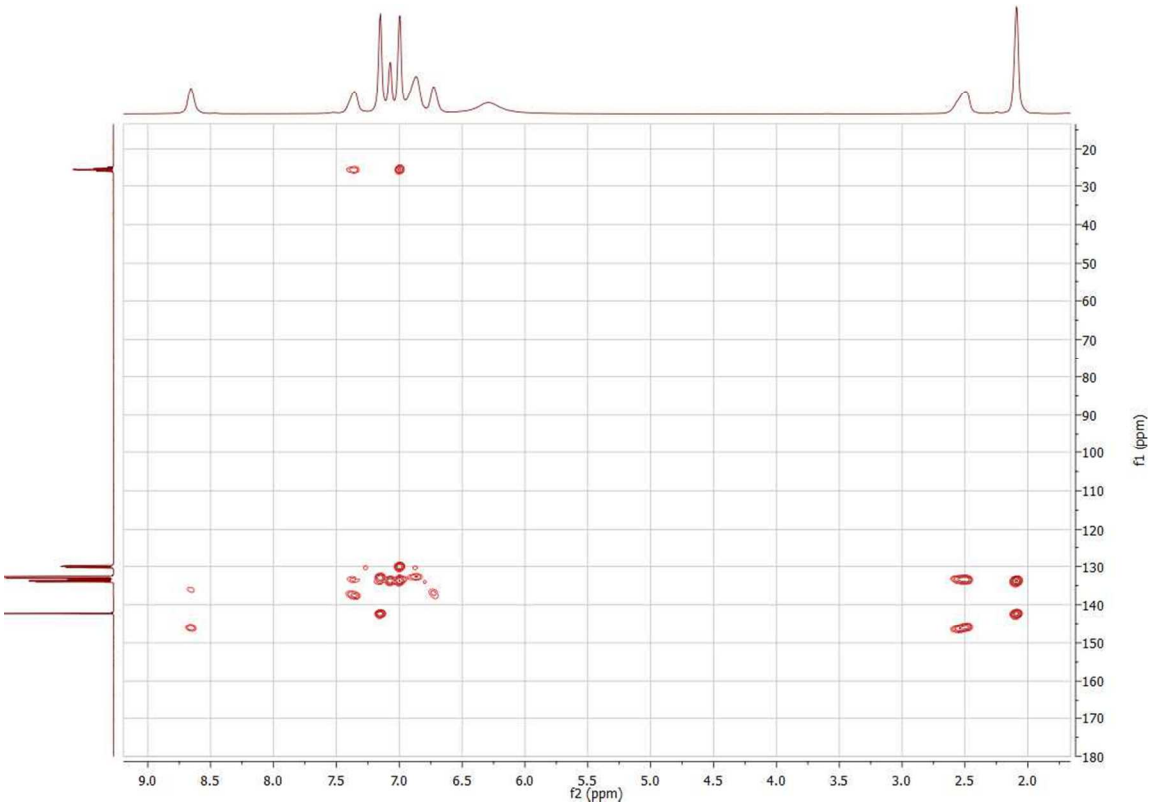

Figure S4. gHMBC NMR spectra of **1** at -60 °C (toluene-d_8 solution).

X-ray crystallography

Suitable crystals of **1** and **2** were mounted on top of a cryoloop and transferred into the cold (100 K) nitrogen stream of a Bruker D8 Venture diffractometer. Data collection and reduction was done using the Bruker software suite APEX2.[4] For compound **1**, data collection was first carried out at 100 K, and when acquisition was complete the crystal was slowly warmed up. Datasets were collected at 400 K, and subsequently at 450 K. The final unit cell was obtained from the xyz centroids of 9838 (**1**, 100 K), 9916 (**1**, 400 K), 7934 (**1**, 450 K) or 9899 (**2**) reflections after integration. A multiscan absorption correction was applied, based on the intensities of symmetry-related reflections measured at different angular settings (*SADABS*).[1] The structures were solved by direct methods using *SHELXS*, and refinement of the structure was performed using *SHLELXL*.[5] For **2**, refinement was frustrated by a disorder problem: two highly disordered THF molecules are present in the asymmetric unit. Ultimately, the contribution from these disordered solvate molecules was removed using the PLATON/SQUEEZE routine.[6] The hydrogen atoms were generated by geometrical considerations, constrained to idealized geometries and allowed to ride on their carrier atoms with an isotropic displacement parameter related to the equivalent displacement parameter of their carrier atoms. Crystal data and details on data collection and refinement are presented in Table S1.

Table S1. Crystallographic data for **1** and **2**

	1 (100 K)	**1** (400 K)	**1** (450 K)	**2**
chem formula	$C_{40}H_{34}FeN_8$	$C_{40}H_{34}FeN_8$	$C_{40}H_{34}FeN_8$	$C_{56}H_{70}FeN_9$
M_r	682.60	682.60	682.60	925.06
cryst syst	monoclinic	monoclinic	monoclinic	monoclinic
color, habit	dark red, block	dark red, block	dark red, block	black, block
size (mm)	0.37 x 0.25 x 0.22	0.37 x 0.25 x 0.22	0.37 x 0.25 x 0.22	0.41 x 0.33 x 0.19
space group	P21/n	P21/n	P21/n	P2/n
a (Å)	8.5794(3)	8.875(3)	11.788(6)	12.1244(7)
b (Å)	11.7518(4)	11.746(3)	15.996(9)	14.1187(8)
c (Å)	33.5114(12)	34.068(9)	19.544(11)	18.1921(10)
β (°)	95.9494(10)	94.516(9)	102.051(17)	93.083(2)
V (Å^3)	3360.5(2)	3540.4(16)	3604(3)	3109.6(3)
Z	4	4	4	2
ρ_{calc}, g.cm^{-3}	1.349	1.281	1.258	0.988
Radiation [Å]	Mo K_α 0.71073	Mo K_α 0.71073	Mo K_α 0.71073	Mo K_α 0.71073
μ(Mo K_α), mm^{-1}	0.491	0.466	0.458	0.280
F(000)	1424	1424	1424	990
temp (K)	100(2)	400(2)	450(2)	100(2)
θ range (°)	2.86 - 27.96	2.88 - 27.21	2.76 - 23.26	2.89 – 27.10
data collected (h,k,l)	-11:11; -15:15; -43:44	-11:11; -15:12; -42:43	-13:13; -17:17; -21:21	-15:14; -18:18; -23:23
no. of rflns collected	36390	37877	40771	62606
no. of indpndt reflns	8027	7848	5153	6851
observed reflns $F_o \geq 2.0$ σ (F_o)	6779	5163	2617	5768
R(F) (%)	4.42	8.99	5.61	6.28
wR(F^2) (%)	9.79	18.22	14.43	14.96
GooF	1.105	1.199	1.023	1.132
weighting a,b	0.0298, 3.7094	0.0576, 2.6090	0.0380, 3.4245	0.0523, 5.4617
params refined	444	444	444	302
min, max resid dens	-0.457, 0.390	-0.238, 0.389	-0.170, 0.254	-0.356, 0.380

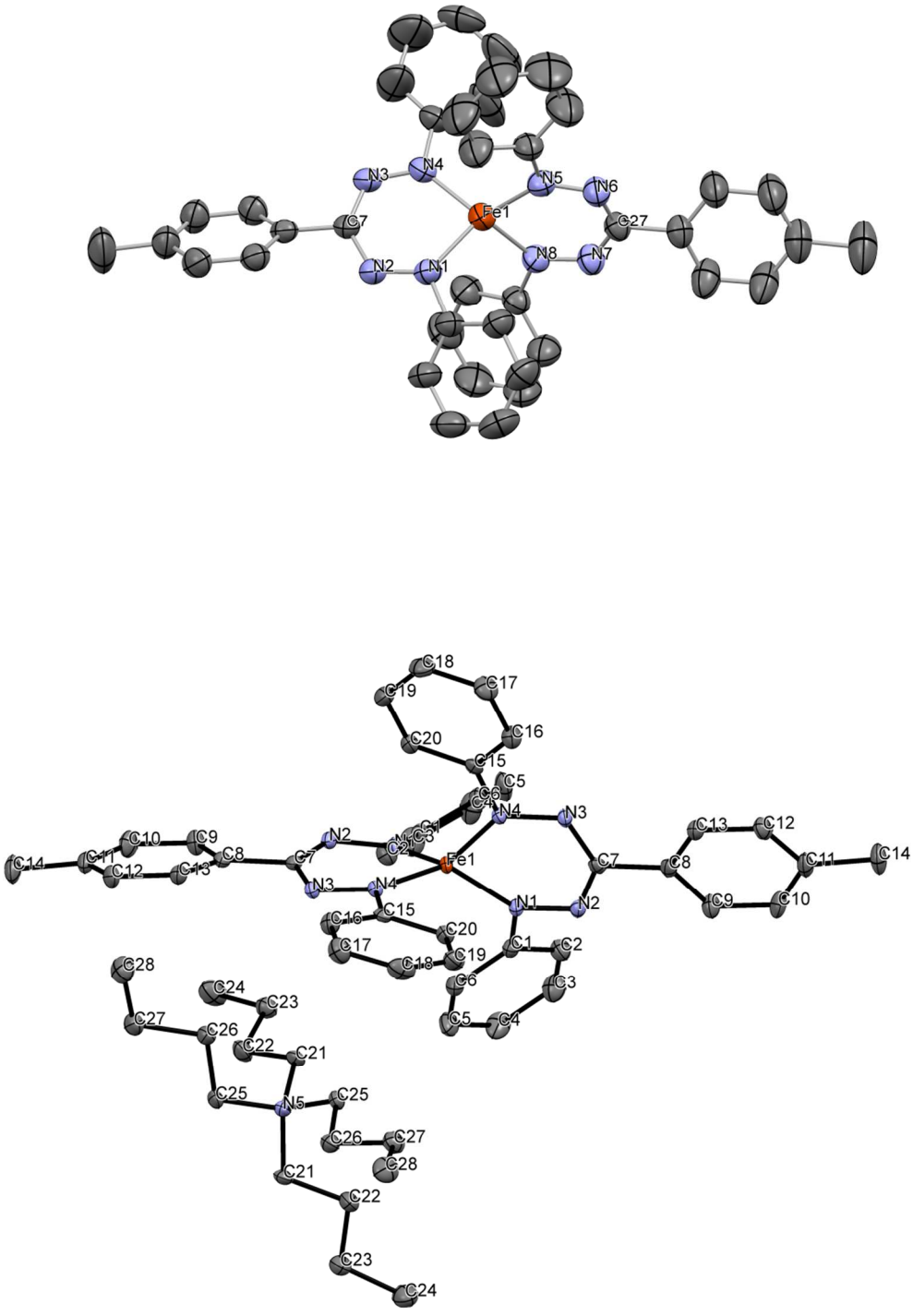

Figure S5. Molecular structures of compound **1** (450 K structure, top) and compound **2** (100 K, bottom), showing 30% and 50% probability ellipsoids, respectively.

Table S2. Pertinent interatomic distances and bond angles in compounds **1** and **2**

	1	**1**	**1**	**2**
	100 K	**400 K**	**450K**	**100K**
Fe(1) – N(1)	1.8278(15)	1.832(3)	1.920(4)	1.8562(19)
Fe(1) – N(4)	1.8207(16)	1.817(3)	1.910(4)	1.8755(19)
Fe(1) – N(5)	1.8330(16)	1.828(3)	1.909(4)	
Fe(1) – N(8)	1.8174(16)	1.821(3)	1.919(4)	
N(1) – N(2)	1.327(2)	1.321(4)	1.303(5)	1.344(3)
N(3) – N(4)	1.329(2)	1.327(4)	1.314(5)	1.347(3)
N(5) – N(6)	1.328(2)	1.317(4)	1.319(5)	
N(7) – N(8)	1.327(2)	1.315(4)	1.303(5)	
N(2) – C(7)	1.343(2)	1.331(5)	1.349(5)	1.341(3)
N(3) – C(7)	1.341(2)	1.330(4)	1.341(5)	1.338(3)
N(6) – C(27)	1.343(2)	1.331(5)	1.339(6)	
N(7) – C(27)	1.338(2)	1.334(5)	1.345(6)	
N(1)–Fe(1)–N(4)	91.24(7)	91.37(13)	91.33(17)	93.84(8)
N(5)–Fe(1)–N(8)	91.36(7)	90.86(13)	91.23(18)	
(N-Fe-N)/(N-Fe-N)	60.97	62.62	77.80	62.26
CShM (T-4)[a]	6.19	5.84	3.20	5.27
CShM (SP-4)[a]	13.47	14.14	21.52	14.44

[a] The continuous shape measure (CShM) calculations provide a measure (distance) between the observed and ideal coordination polyhedron, with smaller values indicating a closer resemblance with that polyhedron (T-4 = tetrahedral; SP-4 = square planar).[7]

Mössbauer spectroscopy

Mössbauer spectra were recorded with a ^{57}Co source in a Rh matrix using an alternating constant acceleration *Wissel* mössbauer spectrometer operated in the transmission mode and equipped with a *Janis* closed-cycle helium cryostat. Isomer shifts are given relative to iron metal at ambient temperature. Simulation of the experimental data was performed with the *Mfit* program: E. Bill, Max-Planck Institute for Chemical Energy Conversion, Mülheim/Ruhr, Germany.

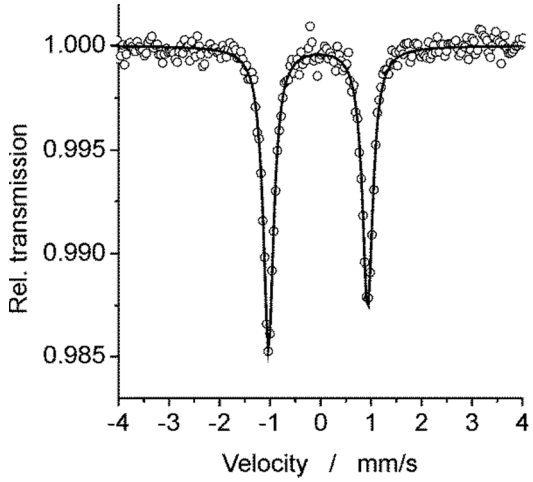

Figure S6. Mössbauer spectrum of **1** in the solid state at 300 K.

Magnetic measurements

Temperature-dependent magnetic susceptibilities were measured by using a SQUID magnetometer (*Quantum Design MPMS XL-5*) in a magnetic field of 0.5 T.

The solid samples were contained in a gel bucket and fixed in a non-magnetic sample holder. Each raw data file for the measured magnetic moment was corrected for the diamagnetic contribution of the gel bucket according to $M^{dia} = \chi_g \cdot m \cdot H$, with experimentally obtained gram susceptibility of gel bucket (χ_g = $-5.70 \cdot 10^{-7}$ emu/(g·Oe)). The molar susceptibility data were corrected for the diamagnetic contribution according to χ_M^{dia}(sample) = $-0.5 \cdot M \cdot 10^{-6}$ cm^3·mol^{-1}. Simulation of the experimental data was performed with the *julX* program: E. Bill, Max-Planck Institute for Chemical Energy Conversion, Mülheim/Ruhr, Germany. Magnetic properties of **2** in solid state were simulated using a Spin-Hamiltonian that includes term for Zeeman splitting: $\hat{H} = g\mu_B \vec{B} \cdot \vec{S}$. Temperature-independent paramagnetism (*TIP*) was included according to $\chi_{calc} = \chi + TIP$ (*TIP* = $80 \cdot 10^{-1}$ cm^{3}mol^{-1} for **1** and $130 \cdot 10^{-1}$ cm^{3}mol^{-1} for **2**).

For the solution measurement solid **1** was dissolved in THF or toluene and the solution was sealed in an NMR-tube.

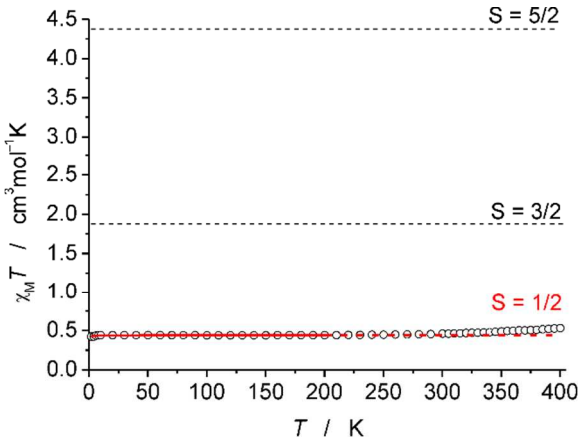

Figure S7. Magnetic susceptibility measurements for **2** in the solid state. The solid red line represents the simulation in the range 2 – 200 K for $S = 1/2$ with $g = 2.17$, the dashed red line represents the curve progression for this simulation up to 400 K. The black dashed lines show spin-only values for hypothetical $S = 3/2$ and $S = 5/2$ spin states.

DSC measurements

Differential scanning calorimetry (DSC) measurements were performed on a Perkin-Elmer DSC-7 equipped with a Perkin-Elmer TAAC 7/DX thermal analysis controller. The sample was sealed in an aluminium pan inside the glovebox and subsequently taken out for analysis. Heating/cooling rates were 10 °C/min. In the first heating cycle (to 175 °C), a sharp endothermic transition was observed at 154.7 °C. Upon cooling to 25 °C, no clear transition was observed. Subsequent heating to 175 °C does not show the initial peak at 154.7 °C. Upon heating the same sample to 250 °C, a broad exothermic transition is observed starting at ca. 205 °C, which is likely due to decomposition of the sample.

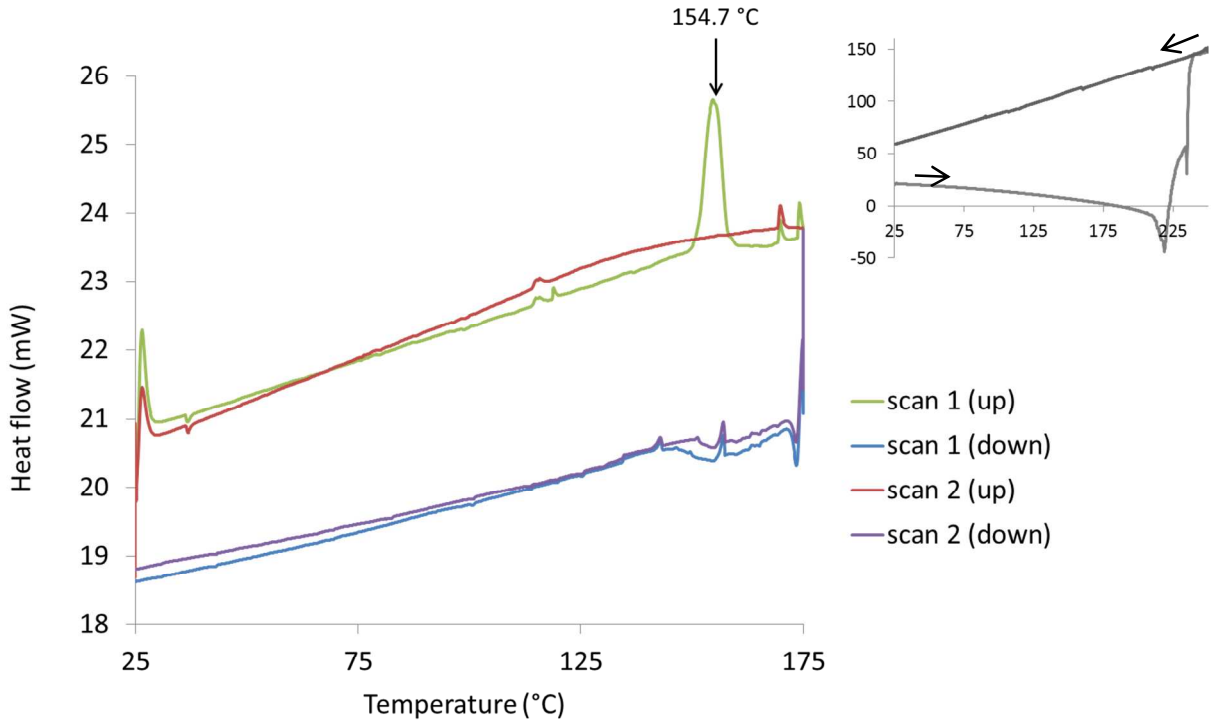

Figure S8. Differential scanning calorimetry measurements for **1**. The inset (top right) shows the results obtained following the initial scans (to 175 °C), but extending the temperature range to 250 °C.

UV/vis absorption spectra

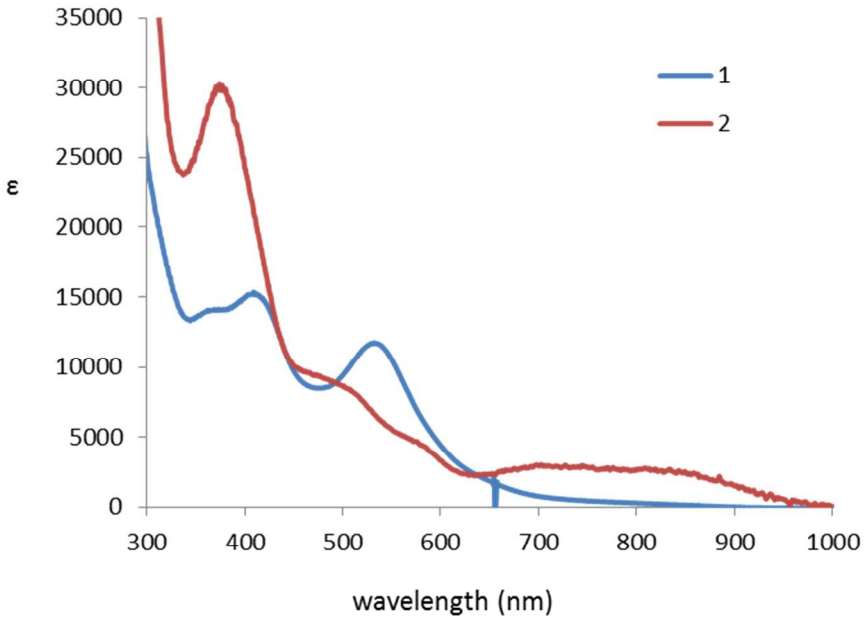

Figure S9. UV/vis absorption spectra of **1** (in toluene) and **2** (in THF) at room temperature.

Variable temperature UV/vis spectra of **1** in toluene were recorded using an Agilent Cary 60 equipped with a Unisoku Cryostat (CoolSpek) and magnetic stirrer using custom-made Schlenk quartz cuvettes. Spectra between 263 and 353 K are shown in Figure S10.

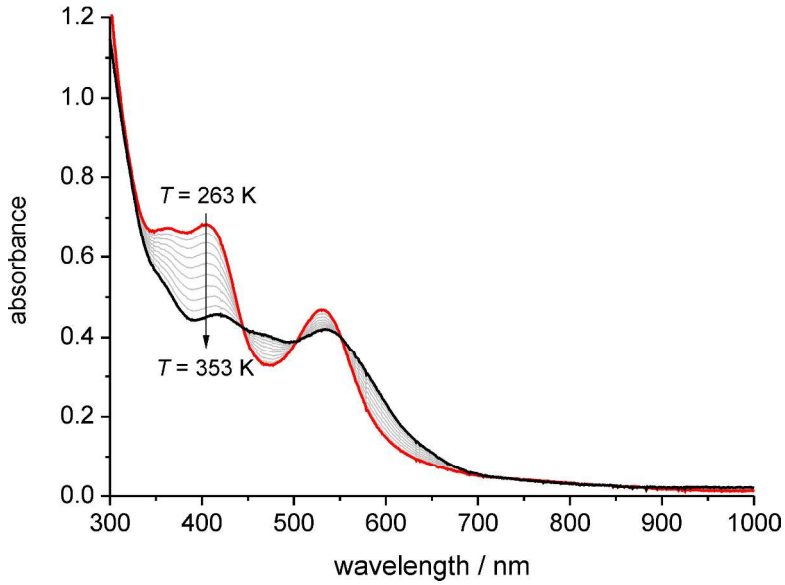

Figure S10. Variable temperature UV/vis spectra of **1** between 263 and 353 K (in toluene, *c* = 0.05 mM) with 10 K steps.

The peak at 405 nm was selected for plotting the molar extinction coefficient ε against temperature (Figure S11).

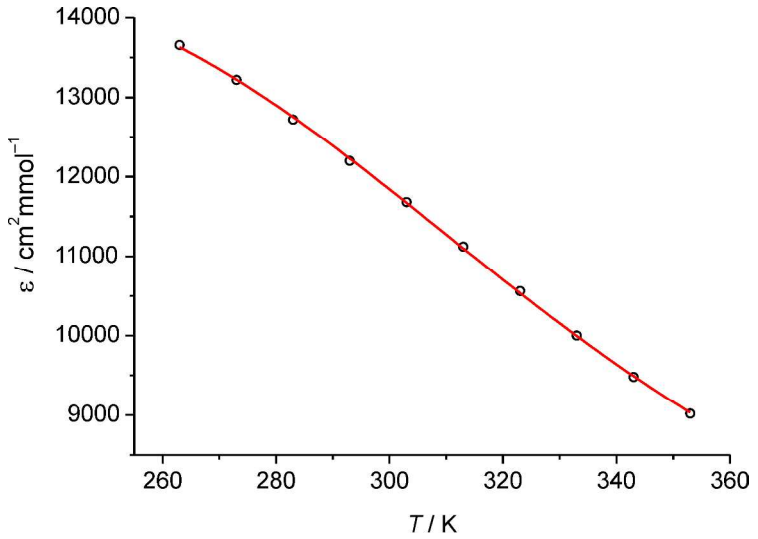

Figure S11. Plot of the molar extinction coefficient ε *vs. T* at 405 nm. The solid line represents the calculated curve fit (see text).

The temperature dependence of the experimentally obtained ε values is attributed to the change of the mole fraction of molecules in the HS state γ_{HS}:

$$\gamma_{HS} = \frac{\varepsilon - \varepsilon_{LS}}{\varepsilon_{HS} - \varepsilon_{LS}} \qquad \text{(eq. 2)}$$

or

$$\varepsilon = \varepsilon_{LS} + \gamma_{HS}(\varepsilon_{HS} - \varepsilon_{LS}) \qquad \text{(eq. 3),}$$

where the ε_{HS} and ε_{LS} are the molar extinction coefficients of the pure HS and LS states.

According to the ideal solution model[2]:

$$\gamma_{HS} = \frac{1}{1 + \exp(\Delta H / RT - \Delta S / R)} \qquad \text{(eq. 4).}$$

Inserting (eq. 4) in (eq. 3) gives an analytical expression for the temperature dependence of extinction coefficient ε:

$$\varepsilon = \varepsilon_{LS} + \left(\frac{1}{1 + \exp(\Delta H / RT - \Delta S / R)}\right)(\varepsilon_{HS} - \varepsilon_{LS}) \qquad \text{(eq. 5).}$$

Since the transition is incomplete, the molar extinction coefficients ε_{HS} and ε_{LS} are unknown and have to be determined from a fit using (eq. 5). Thus, together with thermodynamic parameters ΔH and ΔS, four parameters have to be fitted. To avoid over-parametrization, the ΔS value was fixed to 64 $J \cdot mol^{-1} \cdot K^{-1}$ as derived from NMR experiments. The best fit could then be obtained with the parameters ΔH = 21.1 $kJ \cdot mol^{-1}$, ε_{HS} = 5600 $cm^2 \cdot mmol^{-1}$ and ε_{LS} = 14780 $cm^2 \cdot mmol^{-1}$. The ΔH value is in excellent agreement with the one obtained from NMR experiments (22.2 $kJ \cdot mol^{-1}$). The ε_{HS} and ε_{LS} values can then be used to calculate the mole fraction of molecules in the HS state γ_{HS} (eq. 2). The temperature dependence of γ_{HS} together with the simulated line using (eq. 4) with fit values obtained according to (eq. 5) are depicted in Figure S12. It should be noted that this analysis is an approximation because temperature dependent changes in effective concentration (caused by the change in density of the solvent with temperature) and changes in absorption line shape are neglected.

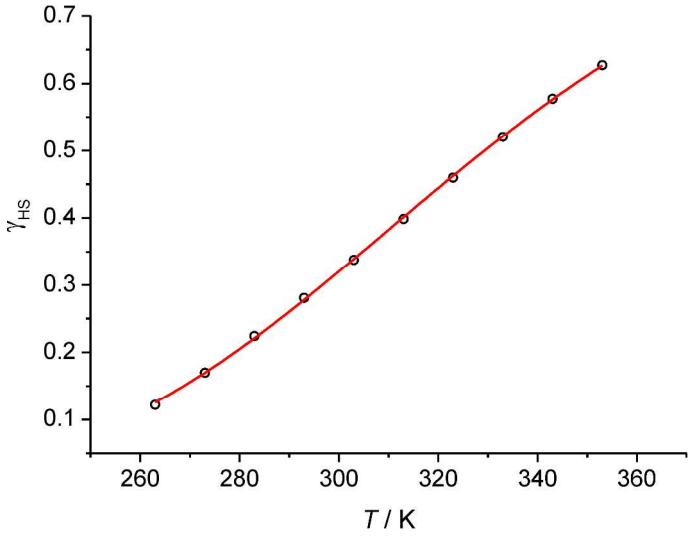

Figure S12. Plot of the mole fraction in the HS state (γ_{HS}) *vs. T*. The solid line represents the simulation using fit parameters described in the text.

Computational studies

Calculations were performed with either the ORCA[8] or Gaussian09[9] program using density functional theory (DFT). Initially, single point calculations (B3LYP/TZVP) were performed using the crystallographic coordinates of **1** to evaluate the relative energy and calculated Mössbauer parameters for the various spin states (Table S3).

Table S3. B3LYP/TZVP energies and DFT-predicted Mössbauer parameters for various spin states of **1** from single-point calculations using the crystallographic coordinates.

	energy (a.u.)	relative energy (kcal/mol)	IS (mm/s)	ΔE_Q (mm/s)
singlet	-3245.279872	1.2	-0.03	-1.93
triplet	-3245.277504	2.6	0.03	-2.14
quintet	-3245.243656	23.9	0.12	1.25
BS11	-3245.281717	0	-0.01	-1.41

Geometry optimizations for the various spin states were carried out using Gaussian09 using the density functionals B3LYP, BP86, OLYP and OPBE (all with the TZVP basis set). The structures were identified as minima on the potential energy surface by frequency calculations (no imaginary frequencies present). Subsequently, these optimized geometries were used to calculate the Mössbauer parameters with ORCA (Table S4). For visualisation of the computed structures and molecular orbitals the program Chemcraft was used.[10]

Table S4. Energies and DFT-predicted Mössbauer parameters for various spin states of **1** using optimized geometries.

		electronic energy (a.u.)	Gibbs free energy (a.u.)	relative electronic energy (kcal/mol)[a]	relative Gibbs free energy (a.u.)[a]	IS (mm/s)	ΔE_Q (mm/s)
singlet	B3LYP	-3247.08691	-3246.51748			0.12	-1.59
	BP86	-3247.30690	-3246.75779			0.03	-1.63
	OLYP	-3246.62928	-3246.07343			0.06	-1.63
	OPBE	-3246.43681	-3245.87894				
triplet	B3LYP	-3247.10131	-3246.53395	-9.0	-10.3	0.38	-1.40
	BP86	-3247.29359	-3246.74834	8.4	5.9	0.31	-1.55
	OLYP	-3246.62506	-3246.07398	2.6	-0.3	0.39	-1.48
	OPBE	-3246.43030	-3245.87720	4.1	1.1		
quintet	B3LYP	-3247.11019	-3246.54698	-14.6	-18.5	0.63	1.42
	BP86	-3247.27938	-3246.73967	17.3	11.4	0.54	1.32
	OLYP	-3246.62703	-3246.07996	1.4	-4.1	0.59	1.47
	OPBE	-3246.43162	-3245.88219	3.3	-2.0		
BS11	B3LYP	-3247.09148	-3246.52013	-2.9	-1.7	0.26	-1.75
	BP86	[b]					
	OLYP	[b]					
	OPBE	[b]					

[a] all energies are relative to the singlet state

[b] calculations converged on a closed-shell singlet state

A single point calculation at the BP86 optimized geometry (S = 2) was performed using ORCA. A corresponding orbital transformation was carried out; the frontier orbitals resulting from this analysis are shown in Figure S7.

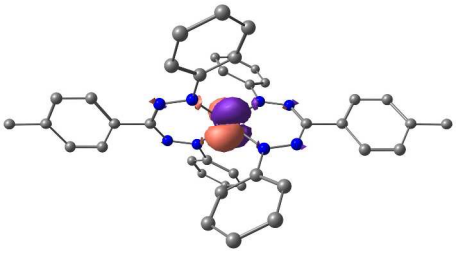

179 (singly occupied)

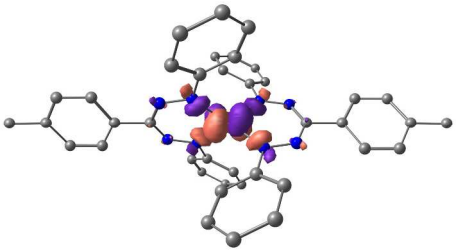

178 (singly occupied)

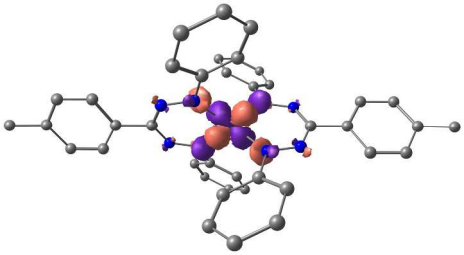

177 (singly occupied)

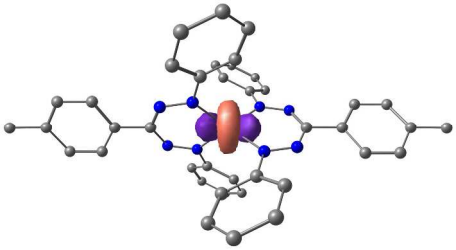

176 (singly occupied)

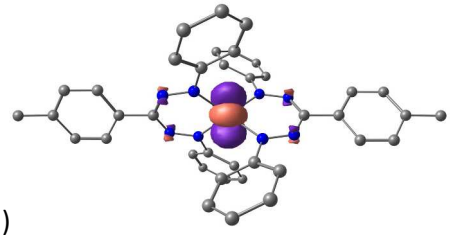

175 (doubly occupied)

Figure S13. Corresponding orbitals from a single point calculation on the S = 2 (BP86/TZVP optimized geometry)

DFT calculations on **2** were performed using B3LYP and BP86 functionals (with TZVP basis set). The energies of various the doublet (S = ½) and broken-symmetry (BS(2,1) and BS(3,2) solutions were calculated, either using the crystallographic coordinates or on the optimized geometries. All broken-symmetry calculations converged to the S = ½ situation, regardless of the functional used.

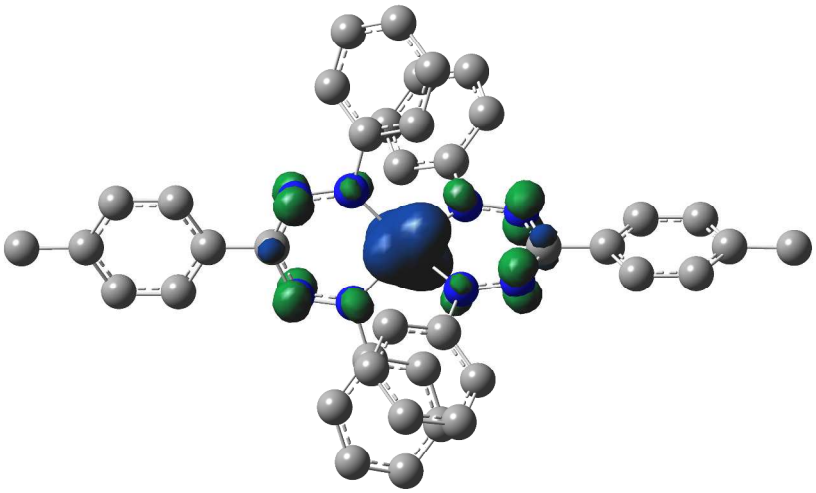

Figure S14. Spin density plot for **2** (BP86/TZVP optimized geometry)

Cyclic voltammetry

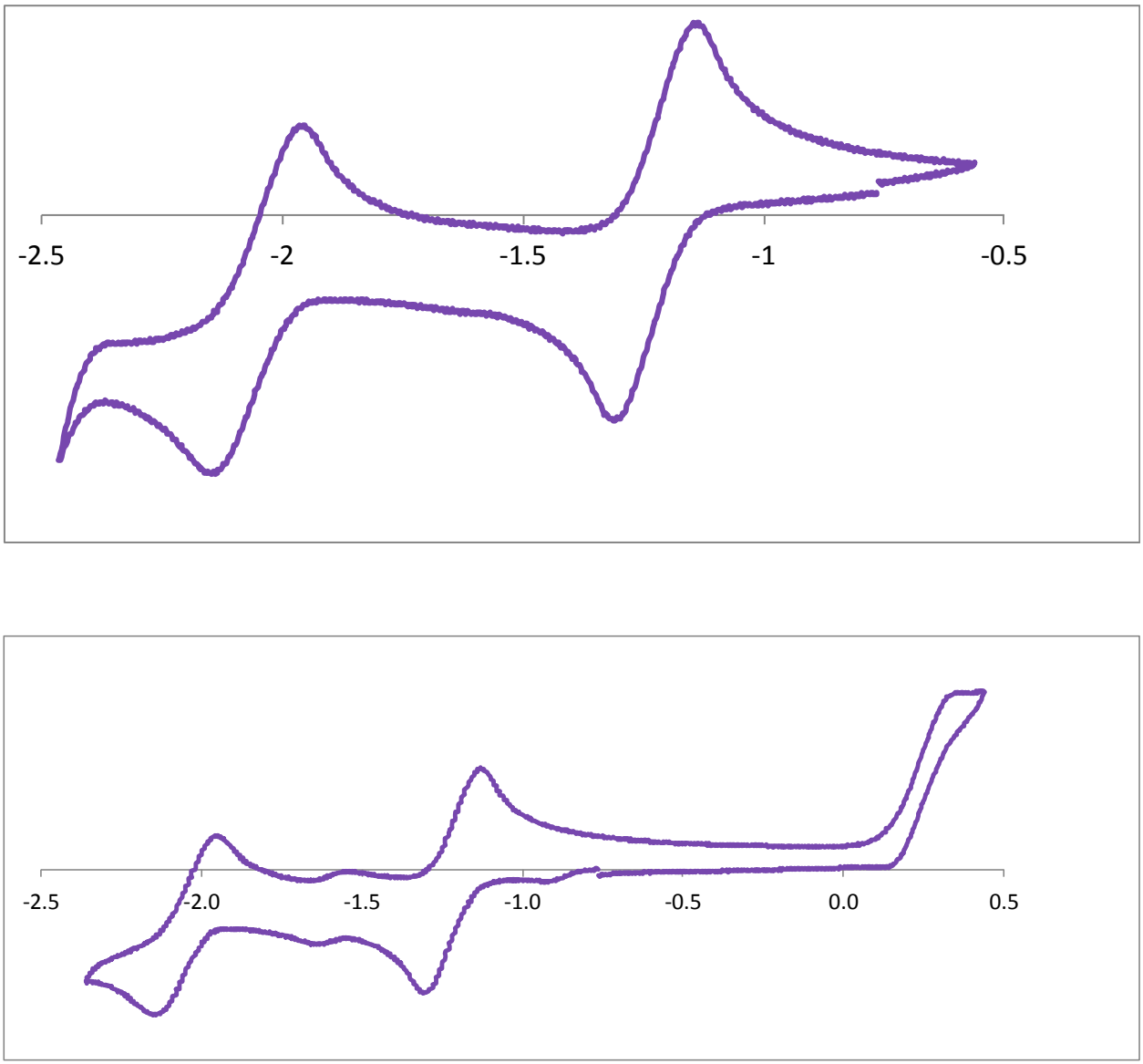

Figure S15. Cyclic voltammetry of **1** recorded at 100 $mV.s^{-1}$ (1.5 mM solution in THF, 0.1 M $[Bu_4N][PF_6]$).

References

(1) Travieso-Puente, R.; Chang, M.-C.; Otten, E. *Dalton Trans.* **2014**, *43*, 18035.

(2) (a) Kläui, W.; Eberspach, W.; Gütlich, P. *Inorg. Chem.* **1987**, *26*, 3977. (b) Lin, H.-J.; Siretanu, D.; Dickie, D. A.; Subedi, D.; Scepaniak, J. J.; Mitcov, D.; Clérac, R.; Smith, J. M. *J. Am. Chem. Soc.* **2014**, *136*, 13326.

(3) Chang, M.-C.; Dann, T.; Day, D. P.; Lutz, M.; Wildgoose, G. G.; Otten, E. *Angew. Chem. Int. Ed.* **2014**, *53*, 4118.

(4) Bruker. *APEX2 (v2012.4-3), SAINT (Version 8.18C) and SADABS (Version 2012/1). Bruker AXS Inc., Madison, Wisconsin, USA.* **2012**.

(5) Sheldrick, G. *Acta Cryst. A* **2008**, *64*, 112.

(6) Spek, A. *J. Appl. Crystallogr.* **2003**, *36*, 7.

(7) Alvarez, S.; Alemany, P.; Casanova, D.; Cirera, J.; Llunell, M.; Avnir, D. *Coord. Chem. Rev.* **2005**, *249*, 1693.

(8) Neese, F. *WIREs Comput. Mol. Sci.* **2012**, *2*, 73.

(9) Solomon, E. I.; Sarangi, R.; Woertink, J. S.; Augustine, A. J.; Yoon, J.; Ghosh, S. *Acc. Chem. Res.* **2007**, *40*, 581.

(10) http://www.chemcraftprog.com.